crystals

MDPI

Article

Room Temperature Synthesis of Various Color Emission Rare-Earth Doped Strontium Tungstate Phosphors Applicable to Fingerprint Identification

Soung-Soo Yi [1] and Jae-Yong Jung [2,*]

[1] Division of Materials Science and Engineering, Silla University, Busan 45985, Korea; ssyi@silla.ac.kr
[2] Research and Business Development Foundation, Engineering Building, Silla University, Busan 45985, Korea
* Correspondence: eayoung21@naver.com; Tel.: +82-50-999-6441

Abstract: Crystalline $SrWO_4$ was synthesized at room temperature using a co-precipitation method. To use the $SrWO_4$ as a phosphor, green and red phosphors were synthesized by doping with Tb^{3+} and Eu^{3+} rare earth ions. The synthesized samples had a tetragonal structure, and the main peak (112) phase was clearly observed. When the sample was excited using the absorption peak observed in the ultraviolet region, $SrWO_4$:Tb^{3+} showed an emission spectrum of 544 nm, and $SrWO_4$:Eu^{3+} showed an emission spectrum of 614 nm. When Tb^{3+} and Eu^{3+} ions were co-doped to realize various colors, a yellow-emitting phosphor was realized as the doping concentration of Eu^{3+} ions increased. When the synthesized phosphor was scattered on a glass substrate with fingerprints, as used in the field of fingerprint recognition, the fingerprint was revealed by green, red, and yellow emissions in response to a UV lamp.

Keywords: $SrWO_4$; phosphors; luminescence; fingerprint

check for updates

Citation: Yi, S.-S.; Jung, J.-Y. Room Temperature Synthesis of Various Color Emission Rare-Earth Doped Strontium Tungstate Phosphors Applicable to Fingerprint Identification. *Crystals* **2022**, *12*, 915. https://doi.org/10.3390/cryst12070915

Academic Editors: Željka Antić and Alessandra Toncelli

Received: 2 June 2022
Accepted: 24 June 2022
Published: 27 June 2022

1. Introduction

Crystalline tungsten has excellent thermal and chemical stability and has been applied in various fields. A material that is thermally and chemically stable has high energy transfer efficiency from tungsten ion to rare earth ion in the rare earth doped phosphor; thus, it is suitable for use as a host material [1–3]. Rare earth (RE) ions doped in the host lattice can generate high intensity emissions and various emission wavelengths, with a narrow bandgap due to energy transfer between the 4*f*-4*f* shells [4–6]. The type and site symmetry of the rare earth ions doped in a thermally and chemically stable host lattice are important factors in the performance of various types of lighting, laser, and display devices [7–9].

It has been reported that the emission wavelength of phosphors used in various types of light devices can vary depending on the type and concentration of the doped rare earth ions, the sintering temperature, crystal grain size, excitation wavelength, and synthesis conditions [10–13]. In particular, the main emission wavelength of the rare earth ions is determined by competition between electric dipole transitions and magnetic dipole transitions. If the electric dipole transition is strong, it reacts sensitively to the local environment around the rare earth ions located in the host lattice, but magnetic dipole transitions are hardly affected by external environmental factors [14–16]. For example, two types of emission wavelengths occur in a phosphor doped with europium (Eu^{3+}) ions. In one emission spectrum, an orange emission (~597 nm) spectrum is generated by the $^5D_0 \rightarrow {}^7F_1$ magnetic dipole transition, and the other is a rare red orange (~620 nm) emission signal from the $^5D_0 \rightarrow {}^7F_2$ electric dipole transition. It is known that either the magnetic dipole transition or the electric dipole transition will become the main transition depending on whether Eu^{3+} rare earth ions located in the host lattice are in the inversion-doping region or not, and this determines the emission wavelength [17–19]. Yu et al. synthesized the $BaWO_4$:Eu^{3+}, Bi^{3+} phosphor powder using a solid-state method and chemical immersion

method and observed that the red emission at 613 nm increased as the doping concentration of Bi^{3+} ions increased [20]. Jung et al. synthesized crystalline $BaWO_4$ by preparing a precursor by co-precipitation and heat-treating it at 800 °C. By doping Dy^{3+}, Tb^{3+}, and Sm^{3+} rare earth ions, phosphors emitting yellow, green, and red were synthesized and applied to anti-counterfeiting [21]. Shinde et al. synthesized $NaCaPO_4$ phosphor doped with Ce^{3+}, Eu^{3+}, and Dy^{3+} rare earth ions using the combustion method. In the case of the Ce^{3+} ion-doped phosphor, an emission wavelength of 367 nm was obtained. Blue light emission at 482 nm ($^4F_{9/2} \rightarrow {}^6H_{15/2}$, magnetic dipole transition) and light emission at 576 nm ($^4F_{9/2} \rightarrow {}^6H_{13/2}$, electric dipole transition) were observed [22].

In this study, crystalline $SrWO_4$ was synthesized at room temperature by co-precipitation. Then, green and red phosphors were synthesized by doping with rare earth ions Tb^{3+} and Eu^{3+}, respectively, and yellow phosphors were synthesized by co-doping the two rare earth ions. The structure of the synthesized phosphor, the size and shape of particles, and their luminescence characteristics were investigated. The synthesized phosphor was reacted with a UV lamp to visualize a fingerprint using the emission color, suggesting that it can be applied to the field of anti-counterfeiting.

2. Materials and Methods

2.1. Synthesis of $SrWO_4$:RE^{3+} by Co-Precipitation at Room Temperature

Starting materials: Strontium acetate ($(CH_3CO_2)Sr$, Sigma-Aldrich, reagent grade), Sodium tungstate ($Na_2WO_4 \cdot 2H_2O$, Sigma-Aldrich, ≥99%), Terbium nitrate ($Tb(NO_3)_3 \cdot {}_xH_2O$, Tb^{3+}, Sigma-Aldrich, 99.999%), Europium nitrate ($Eu(NO_3)_3 \cdot 6H_2O$, Eu^{3+}, Sigma-Aldrich, 99.9%)

The synthesis process was as follows. First 1 mmol $(CH_3CO_2)Sr$ was placed in beaker 'A' and stirred with 50 mL distilled water. Then, 1 mmol $Na_2WO_4 \cdot 2H_2O$ was placed in beaker 'B' and stir with 50 mL distilled water (Figure 1). When the solutions in the 'A' and 'B' beakers are completely dissolved and become transparent, pour the 'B' solution into the 'A' beaker, and stir at room temperature for about 20 min. The reacted solutions change to a white opaque color and a powder is formed. The formed powder is recovered by centrifugation at 4000 rpm for 10 min. The recovered powder is washed 3 times with distilled water to remove unreacted substances and then centrifuged again to recover the powder and dried at 80 °C for 16 h (Figure 1). To synthesize the phosphor, 0.25 mmol each of Tb^{3+} and Eu^{3+} was added to the 'A' beaker and processed in the same manner. White light phosphor was synthesized by co-doping by fixing the amount of Tb^{3+} and controlling the amount of Eu^{3+}.

2.2. Fabricated Fingerprint Identification Application

To use the synthesized phosphor for fingerprint recognition, a thumb fingerprint was imprinted on a glass substrate. After spraying the synthesized phosphor on the glass substrate and removing the remaining powder with a brush, the fingerprint on the glass substrate could be visualized by illuminating it with a UV lamp, which revealed the unique luminous color of the phosphor.

2.3. Characterization

The crystal structure of the synthesized phosphor powder was measured using an X-ray diffraction apparatus (X'Pert PRO MPD, 40 kV, 30 mA) having Cu–Kα radiation (wavelength: 1.5406 Å) at a scan rate of 4° per minute at a diffraction angle of 10° to 70°. The size and microscopic surface shape of the crystal grains were photographed with a scanning electron microscope (TESCAN MIRA 3 LMH FE-SEM, TESCAN, Brno, Czech Republic), and a fluorescence photometer (FS-2, Scinco) with a xenon lamp was used as a light source to obtain emission and absorption characteristics.

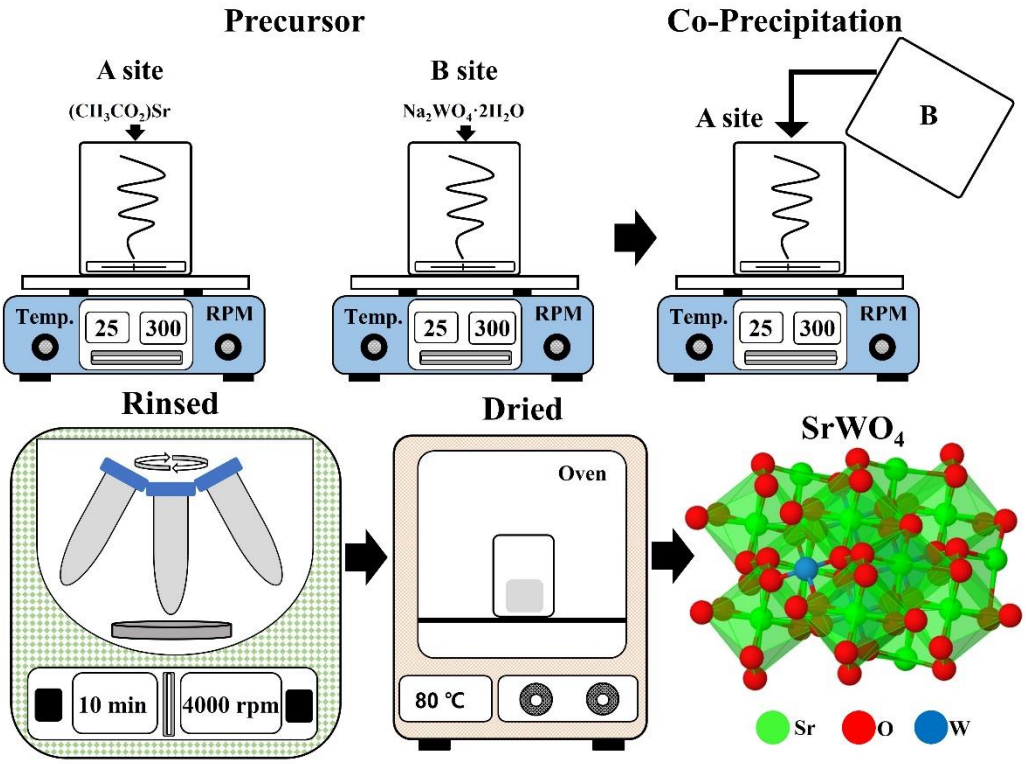

Figure 1. Procedure for co-precipitation.

3. Results & Discussion

3.1. Characteristics of $SrWO_4$ and $SrWO_4$:RE^{3+}

Figure 2a shows the XRD measurement results of $SrWO_4$, $SrWO_4$:Tb^{3+}, and $SrWO_4$:Eu^{3+}. $SrWO_4$ synthesized by co-precipitation showed a tetragonal (a = 5.400 Å, b = 5.400 Å, c = 11.910 Å) structure consistent with ICDD # 01-089-2568. The (112) peak, which is the main diffraction peak, was clearly observed, and the sample to which the rare earth was added also clearly exhibited the main peak.

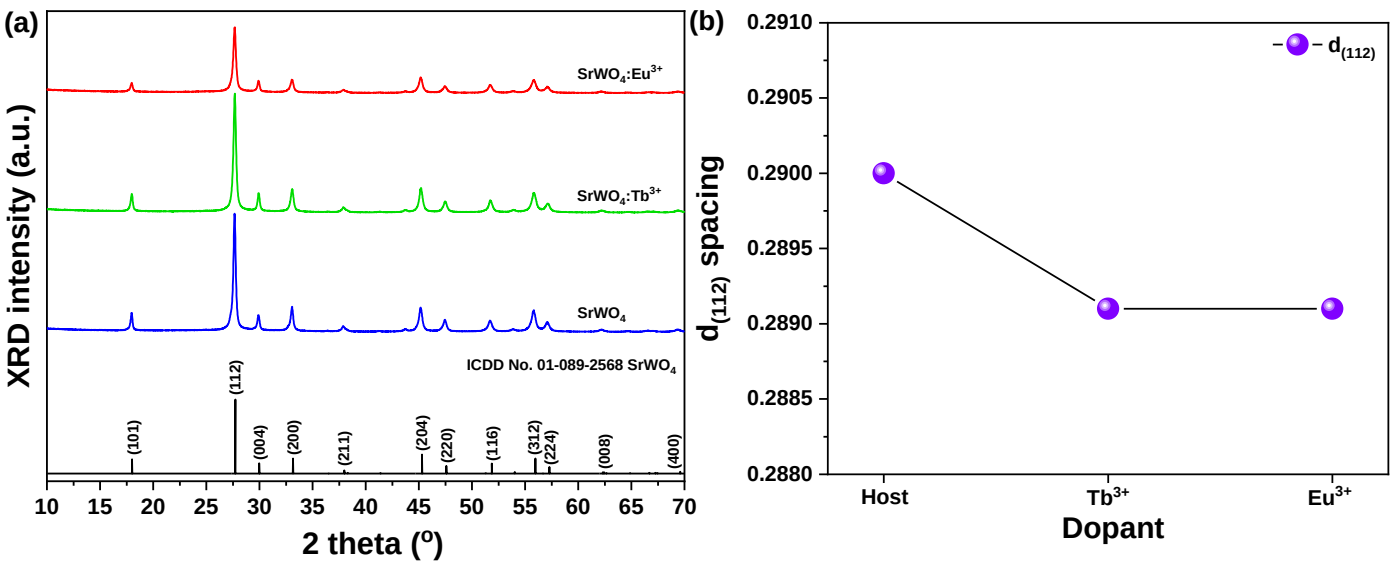

Figure 2. (**a**) XRD patterns, (**b**) $d_{(112)}$ spacing of $SrWO_4$ and $SrWO_4$:RE^{3+}.

Based on the 'Lewis's acid–base' reaction, the samples synthesized by the co-precipitation method showed an explosive reaction when the solution dissolved in beaker 'A' became

'Homo' and the solution dissolved in beaker 'B' became 'Lumo' [23,24], and crystalline $SrWO_4$ was easily synthesized at room temperature. Figure 2b shows the lattice constant change with and without rare earth doping with the (112) plane, which is the main peak of the sample, of the hosts $SrWO_4$, $SrWO_4$:Tb^{3+} and $SrWO_4$:Eu^{3+}, respectively. The lattice constant of the (112) phase, which is the main peak of $SrWO_4$, was slightly changed by the rare earth doping ($SrWO_4$: 0.291 nm, $SrWO_4$:Tb^{3+}: 0.2892 nm, $SrWO_4$:Eu^{3+}: 0.2892 nm). It is considered that the change in the crystal lattice is due to the doping with rare earth ions, which have a relatively large ionic radius [25]. FE-SEM images of the synthesized samples are shown in Figure 3. The samples showed a long cylindrical shape with and without doping.

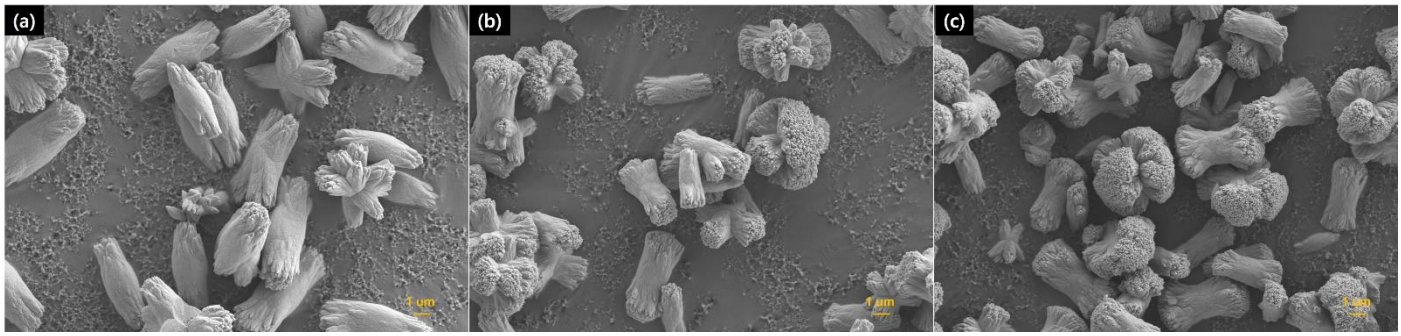

Figure 3. FE-SEM images of (**a**) $SrWO_4$, (**b**) $SrWO_4$:Tb^{3+}, and (**c**) $SrWO_4$:Eu^{3+} samples.

The particle size of $SrWO_4$ was about 5.78 μm in the longitudinal direction and about 2.36 μm in the transverse direction (Figure 3a). Rare earth doped $SrWO_4$:Tb^{3+} particles were about 3.57 μm in the longitudinal direction and about 2.29 μm in the transverse direction (Figure 3b), and $SrWO_4$:Eu^{3+} particles had a size of about 4.82 μm in the longitudinal direction and about 2.31 μm in the transverse direction (Figure 3c). Krishna at al. reported $BaMoO_4$ is synthesized by reacting with $MoO_4{}^{-2}$, which is a monomer of oxyanion and grows in the vertical direction immediately after mixing the Ba aqueous solution and Mo aqueous solution. It is reported that the shape of the shuttle was clearly visible due to the larger rift in Oswald. It was synthesized using basic materials and explained by the action of the bases [26].

The host $SrWO_4$ showed absorption in a wide range, from 220 to 340 nm, and peaked at 277 nm. When the sample was excited at the highest peak of 277 nm, it was broad from 350 to 650 nm, and the peak at 492 nm showed blue–white emission spectrum (Figure 4a). Figure 4b shows the emission spectrum of $SrWO_4$:Tb^{3+} phosphor synthesized by doping Tb^{3+} rare earth ions into $SrWO_4$. The absorption spectrum of the phosphor powder under 544 nm showed that the band of charge-transfer transition (CTB) generated between the O^{-2} and W^{6+} of the $WO_4{}^{2-}$ groups was widely distributed in the 210~290 nm region with a peak at 254 nm [27]. When the phosphor powder was excited with 254 nm, peaks at 487, 544, 586, 620, and 649 nm were observed in the emission spectrum. Among these peaks, the intensity of the green emission spectrum produced by the magnetic dipole transition was the strongest. This emission intensity was 2.99 times stronger than the blue emission intensity produced by the electric dipole transition. The Tb^{3+} ion in the $SrWO_4$ lattice is located at the inversion symmetric site because the emission intensity due to the magnetic dipole transition of green emission is strong [28].

Figure 4c shows the absorption and emission spectrum of the $SrWO_4$:Eu^{3+} phosphor synthesized by doping with the rare earth ion Eu^{3+}. The absorption spectrum of the phosphor powder under 614 nm shows the absorption spectrum by CTB generated between O^{2-} and Eu^{3+} ions, which appear over the 230~310 nm region and have a peak at 277 nm, with Eu^{3+} observed over the 310~400 nm region. Absorption signals due to the 4*f*-4*f* transition of ions were observed [29]. The emission spectrum of the synthesized phosphor was measured by excitation at 277 nm. The phosphor powder showed a red–orange

emission spectrum with a peak emission intensity at a wavelength of 614 nm and a spectrum with peaks at 590, 650, and 700 nm. Among these peaks, the 614 nm peak due to the electric dipole transition and the 590 nm peak due to the magnetic dipole transition signal had an intensity difference of about 7.94 times, indicating that the Eu^{3+} ions in the host are located in non-inversion symmetric sites [30].

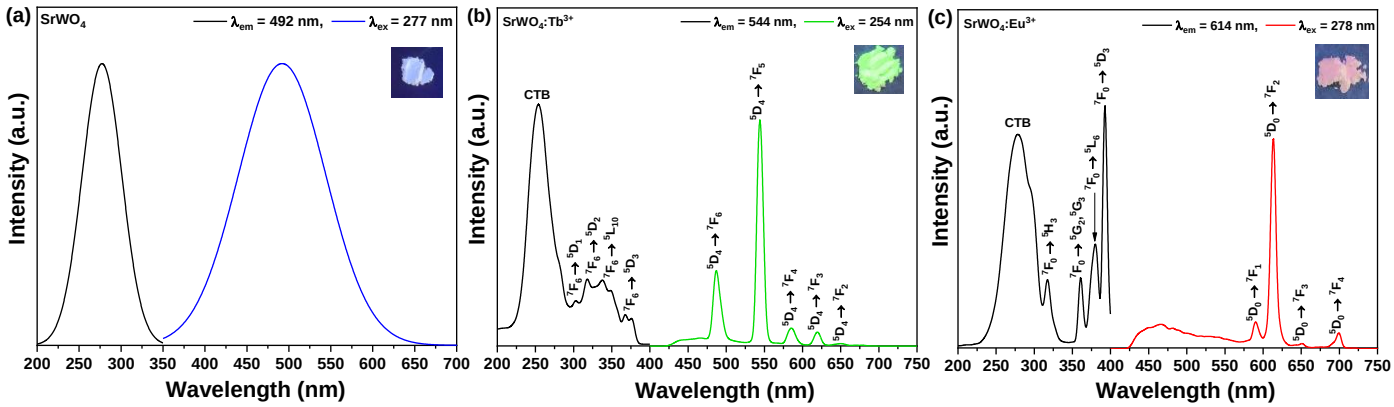

Figure 4. Photoluminescence spectra of (**a**) $SrWO_4$, (**b**) $SrWO_4$:Tb^{3+}, and (**c**) $SrWO_4$:Eu^{3+} samples.

3.2. Characteristics of the $SrWO_4$: [Eu^{3+}]:[Tb^{3+}] Phosphors

Figure 5a shows the X-ray diffraction peak of $SrWO_4$ co-doped with rare earth ions Tb^{3+} and Eu^{3+} as a white light-emitting phosphor. In the XRD pattern of the synthesized samples, a secondary phase caused by rare earth doping was not found, and the diffraction signal of the main peak (112) was clearly observed. Figure 5b shows the lattice constant change of the (112) phase, which is the main peak of the rare earth co-doped $SrWO_4$:[Eu^{3+}]/[Tb^{3+}] samples. Previously, the lattice constants of the $SrWO_4$:Tb^{3+} and $SrWO_4$:Eu^{3+} samples doped with a single rare earth decreased, but the lattice constants of the samples doped with both increased. It is believed that the crystal lattice is distorted, or the structure is changed by the amount of added rare earth ions, which have a relatively large ionic radius.

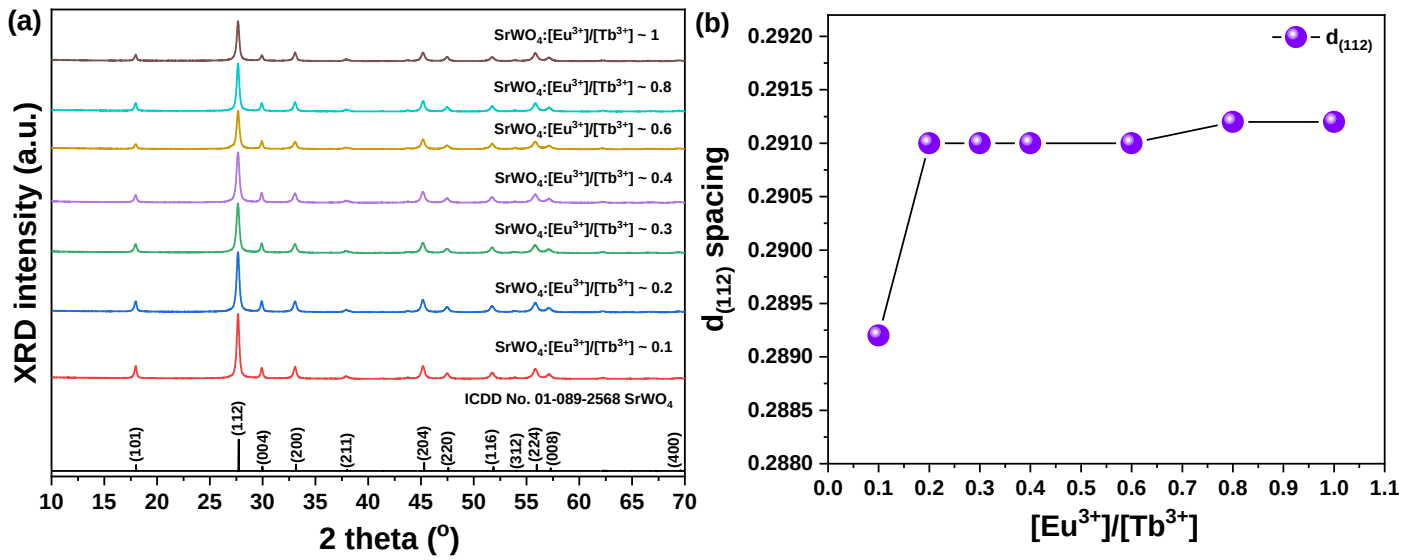

Figure 5. (**a**) XRD patterns of $SrWO_4$:[Eu^{3+}]/[Tb^{3+}] and (**b**) change of $d_{(112)}$ spacing.

Figure 6 shows the FE-SEM images and energy dispersive X-ray spectroscopy (EDS) mapping component analysis results of the synthesized $SrWO_4$:[Eu^{3+}][Tb^{3+}] phosphor. The shape of the particles grew in the longitudinal direction with a cylindrical shape close to the shape of a dumbbell. The particles were about 3.18 μm in the longitudinal direction

and about 1.45 μm in the transverse direction. In the EDS component analysis, Sr, W, O, Tb, and Eu components were detected, which confirmed that rare earth ions had been successfully doped.

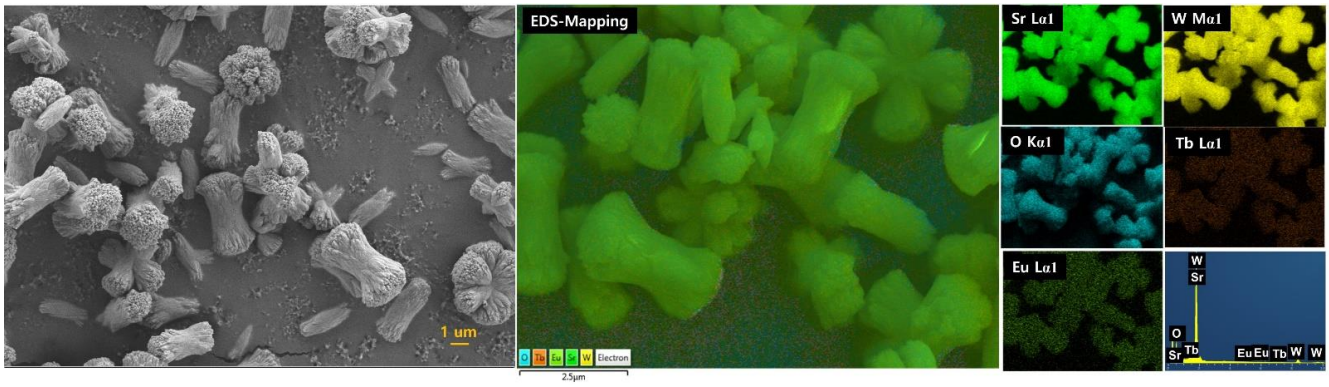

Figure 6. FE-SEM images and EDS mapping analysis of $SrWO_4$:[Eu^{3+}]/[Tb^{3+}].

Figure 7a shows the emission spectrum of the $SrWO_4$:[Eu^{3+}]/[Tb^{3+}] phosphor powder co-doped with changing Eu^{3+} ion concentrations, while the Tb^{3+} ion concentration remained fixed. The emission spectra of the two rare earth ions were shown when excited at a wavelength of 254 nm, as the doping concentration of Eu^{3+} increased. Green at 544 nm and orange–red at 614 nm were simultaneously observed. As the concentration of Eu^{3+} ions increased, the intensity of the green emission by Tb^{3+} ions decreased, which means that the emission energy was converted from Tb^{3+} ions in the host lattice to Eu^{3+} ions (Figure 7b). The energy transfer efficiency from Tb^{3+} to Eu^{3+} ions can be expressed by Equation (1) [31].

$$\eta = 1 - I/I_0 \tag{1}$$

Here, I is the emission intensity of the Tb^{3+} ions in the $SrWO_4$:[Eu^{3+}]/[Tb^{3+}] phosphors, and I_0 is the emission intensity of Tb^{3+} ions in the $SrWO_4$:Tb^{3+} phosphors. As shown in Figure 7c, as the amount of added Eu^{3+} ions increases, the energy transfer efficiency tends to increase. However, the emission intensity decreased, which is a concentration-quenching phenomenon due to excessive rare earth doping [23]. In the CIE color coordinates, as the doping concentration of Eu^{3+} ions increased, the green coordinates moved to the yellow region (Figure 7d). According to Zhu et al. [32], among the Tb^{3+} and Eu^{3+} rare earth ions co-doped with the $CaCO_3$ cubic structure, the green emission of Tb^{3+} decreases and the intensity of the red emission of Eu^{3+} increases as the doping concentration of Eu^{3+} increases. Regarding the energy from Tb^{3+} to Eu^{3+} ions, it was reported that a transfer occurred. In this study, as the doping concentration of Eu^{3+} ions increased in the Tb^{3+} and Eu^{3+} ions co-doped with $SrWO_4$, the intensity of green emission decreased, and the intensity of red emission increased as the energy transfer occurred.

Figure 8 shows the schematic energy diagram of terbium and europium ions luminescence mechanisms in $SrWO_4$:[Eu^{3+}]/[Tb^{3+}] phosphors. The phosphors under 254 nm were excited, and $^5D_3$ states of Tb^{3+} can luminesce non-radiatively to the energetically lower $^3D_4$ excited states. Since the $^5D_4$ states of the Tb^{3+} and the $^5D_3$ states of Eu^{3+} are energetically closed to each other, excitation energy availability transferred to the $^5D_3$ states from Eu^{3+} by the path of resonance transmission. Thus, Tb^{3+} mainly emitted green peaks due to $^5D_4 \rightarrow {}^7F_5$, and Eu^{3+} emitted red due to $^5D_0 \rightarrow {}^7F_J$ [32].

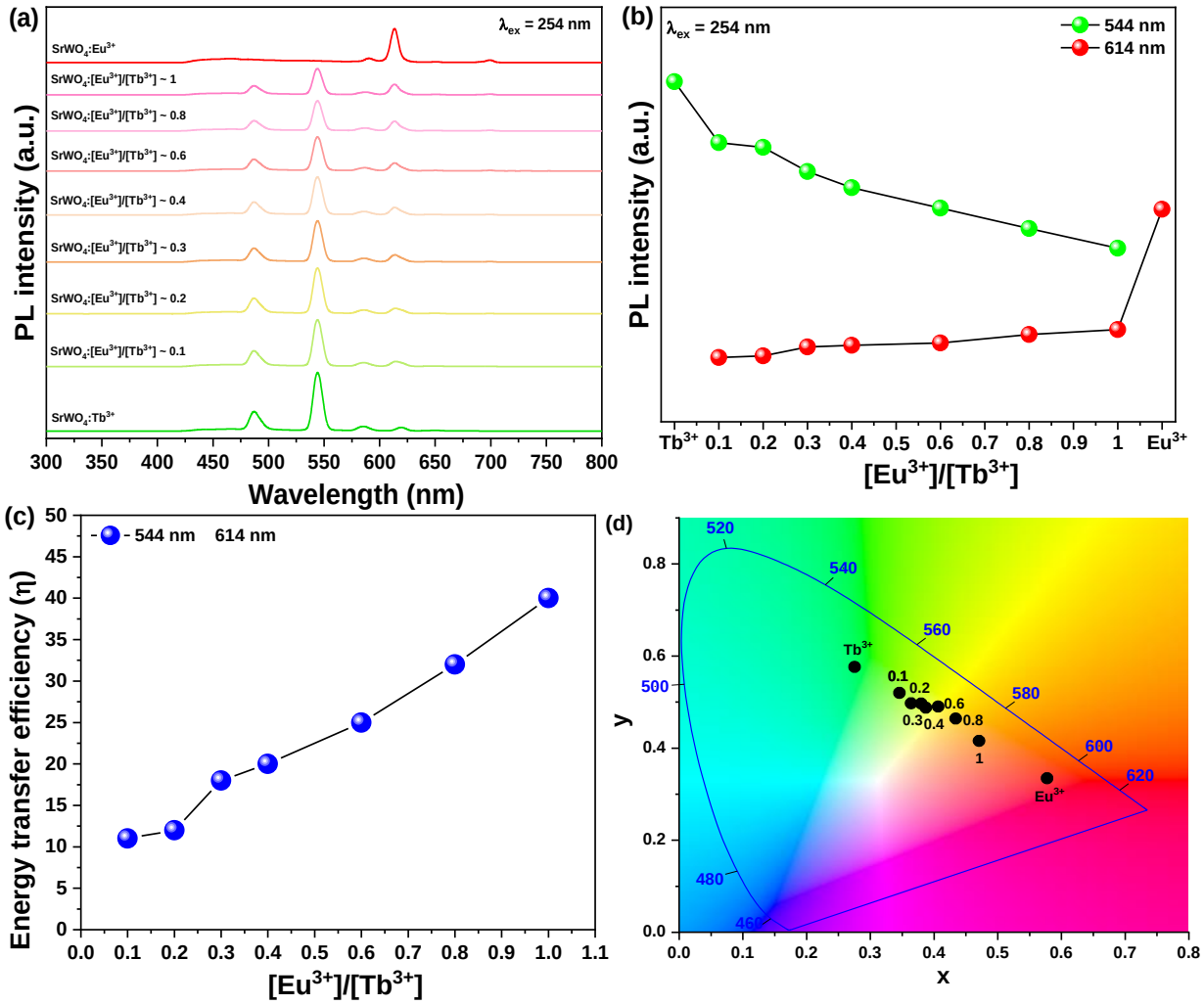

Figure 7. (**a**) Pl spectra under 254 nm, (**b**) change in PL intensity, (**c**) energy transfer efficiency, and (**d**) CIE coordination $SrWO_4$:[Eu^{3+}]/[Tb^{3+}].

Table 1 shows a reported phosphor synthesized by adding various rare earth ions, with tungsten oxide as a host. Several types of phosphors have been reported, such as up-conversion pre-conversion phosphors co-doped with Yb^{3+} and Er^{3+} and red phosphors co-doped with Eu^{3+} and Sm^{3+}. A phosphor was synthesized, and a yellow-emitting phosphor was synthesized by co-doping with Tb^{3+} and Eu^{3+} ions to produce various light-emitting materials as in the previously reported research [33–37].

Table 1. Comparison of previous work in tungsten oxide phosphors.

No.	Host	Rare Earth	Type	Wavalength (nm)
1 [33]	$SrWO_4$	Er^{3+}/Yb^{3+}	Up conversion	489, 525
2 [34]	$SrWO_4$	Tm^{3+}/Yb^{3+}	Up conversion	684, 814
3 [35]	$CaWO_4$	Sm^{3+}/Eu^{3+}	Down conversion	592, 615
4 [36]	$CaWO_4$	Eu^{3+}/Sm^{3+}	Down conversion	622, 630
5 [37]	$SrWO_4$	Eu^{3+}/Sm^{3+}	Down conversion	590, 613
This work	$SrWO_4$	Eu^{3+}/Tb^{3+}	Down conversion	544, 614

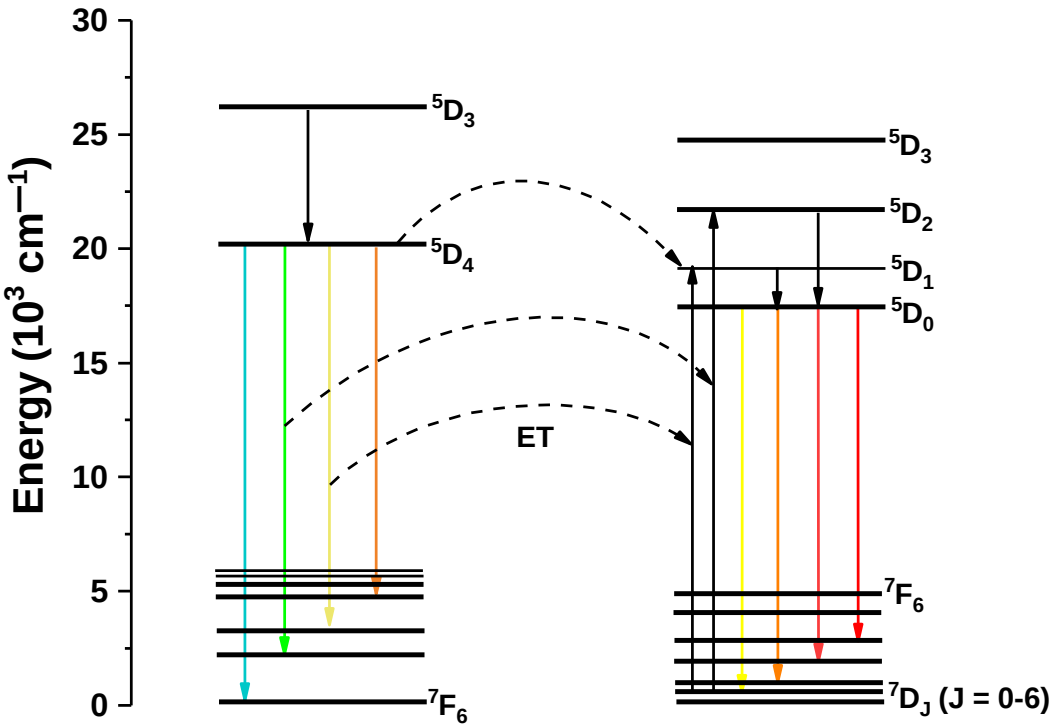

Figure 8. Schematic of Tb^{3+} and Eu^{3+} energy levels indicating the energy transfer processes in the $SrWO_4$ phosphors.

3.3. Applied for Fingerprint Identification

To clearly observe the fingerprint of the author's thumb on the glass substrate, the synthesized phosphor powder was scattered, and then the shape of the fingerprint was visualized by illuminating it with a UV lamp. The phosphor doped with rare earth ions revealed the fingerprints in emissions of green and red, which are their own colors, and the specimens co-doped with Eu^{3+} and Tb^{3+} revealed the fingerprints by emitting yellow light. The results suggest that the synthesized phosphor can be used for fingerprint identification (Figure 9).

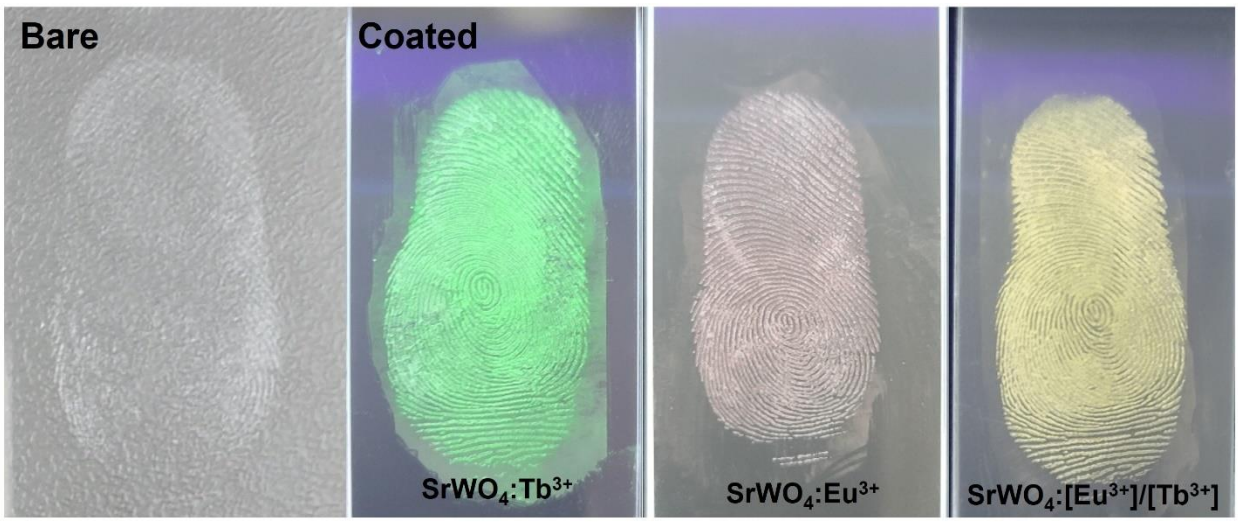

Figure 9. Images of fingerprint coated with phosphors under a UV lamp.

4. Conclusions

Crystalline $SrWO_4$ was synthesized at room temperature by co-precipitation. Then, green and red phosphors were synthesized by doping with rare earth ions, Tb^{3+} and Eu^{3+}, respectively. The synthesized samples clearly exhibited the (112) phase, which was the main peak in the X-ray diffraction pattern, and the lattice constant was changed by doping with rare earth ions. The synthesized specimens had a size of several microns and a cylindrical shape. In addition, when each specimen was excited using an absorption peak in the ultraviolet region, $SrWO_4$:Tb^{3+} exhibited green, and $SrWO_4$:Eu^{3+} emitted red due to the doped rare earth. In the specimen co-doped with Tb^{3+} and Eu^{3+} to obtain various color emissions, the color coordinates shifted to the yellow region as the doping concentration of Eu^{3+} ions increased. The synthesized phosphor was scattered on the glass substrate on which the fingerprint was printed, and when a UV lamp was lit, the green, red, and yellow emission colors were visualized so that the fingerprint could be clearly recognized.

Author Contributions: Conceptualization, J.-Y.J.; methodology, J.-Y.J.; software, J.-Y.J.; validation, J.-Y.J. and S.-S.Y.; formal analysis, J.-Y.J.; investigation, J.-Y.J.; resources, J.-Y.J.; data curation, J.-Y.J.; writing—original draft preparation, J.-Y.J. and S.-S.Y.; writing—review and editing, J.-Y.J. and S.-S.Y.; visualization, J.-Y.J.; supervision, J.-Y.J.; project administration, S.-S.Y. and J.-Y.J.; funding acquisition, S.-S.Y. All authors have read and agreed to the published version of the manuscript.

Funding: This research was supported by the Basic Research Program through the National Research Foundation of Korea (NRF) funded by the Ministry of Education (NRF-2020R1F1A1072676).

Data Availability Statement: The data presented in this study are available on request from the corresponding author.

Conflicts of Interest: The authors declare no conflict of interest.

References

1. Do, Y.R.; Huh, Y.D. Optical Properties of Potassium Europium Tungstate Phosphors. *J. Electrochem. Soc.* **2000**, *147*, 4385–4388. [CrossRef]
2. Zhao, Y.; Wang, X.; Zhang, Y.; Li, Y.; Yao, X. Winning wide-temperature-range and high-sensitive thermometry by a multichannel strategy of dual-lanthanides in the new tungstate phosphors. *J. Alloys Compd.* **2020**, *834*, 154998. [CrossRef]
3. LEE, G.; KIM, T.; YOON, C.; KANG, S. Effect of local environment and Sm^{3+}-codoping on the luminescence properties in the Eu^{3+}-doped potassium tungstate phosphor for white LEDS. *J. Lumin.* **2008**, *128*, 1922–1926. [CrossRef]
4. Hua, Y.; Yu, J.S. Double-excited states of charge transfer band and 4f-4f in single-phase $K_3Gd(VO_4)_2$:Tb^{3+}/Sm^{3+} phosphors with superior sensing sensitivity for potential luminescent thermometers. *J. Mater. Sci. Technol.* **2021**, *91*, 148–159. [CrossRef]
5. Qin, X.; Liu, X.; Huang, W.; Bettinelli, M.; Liu, X. Lanthanide-Activated Phosphors Based on 4f-5d Optical Transitions: Theoretical and Experimental Aspects. *Chem. Rev.* **2017**, *117*, 4488–4527. [CrossRef]
6. Li, L.; Yang, P.; Xia, W.; Wang, Y.; Ling, F.; Cao, Z.; Jiang, S.; Xiang, G.; Zhou, X.; Wang, Y. Luminescence and optical thermometry strategy based on emission and excitation spectra of Pr^{3+} doped $SrMoO_4$ phosphors. *Ceram. Int.* **2021**, *47*, 769–775. [CrossRef]
7. Wu, H.; Niu, P.; Pei, R.; Zheng, Y.; Jin, W.; Li, X.; Jiang, R. Tb^{3+} and Sm^{3+} co-doped $CaWO_4$ white light phosphors for plant lamp synthesized via solid state method: Phase, photoluminescence and electronic structure. *J. Lumin.* **2021**, *236*, 118146. [CrossRef]
8. Pollnau, M.; Romanyuk, Y.E.; Gardillou, F.; Borca, C.N.; Griebner, U.; Rivier, S.; Petrov, V. Double Tungstate Lasers: From Bulk Toward On-Chip Integrated Waveguide Devices. *JSTQE* **2007**, *13*, 661–671. [CrossRef]
9. Semenov, P.A.; Meshchanin, A.P.; Davidenko, A.M.; Kormilitsin, V.A.; Batarin, V.A.; Goncharenko, Y.M.; Stone, S.; Kravtsov, V.I.; Matulenko, Y.A.; Semenov, V.K.; et al. Design and performance of LED calibration system prototype for the lead tungstate crystal calorimeter. *Nucl. Instrum. Methods Phys. Res. Sect. A Accel. Spectrometers Detect. Assoc. Equip.* **2005**, *556*, 94–99. [CrossRef]
10. Jung, J.-Y. Luminescent Color-Adjustable Europium and Terbium Co-Doped Strontium Molybdate Phosphors Synthesized at Room Temperature Applied to Flexible Composite for LED Filter. *Crystals* **2022**, *12*, 552. [CrossRef]
11. Feng, L.; Chen, X.; Mao, C. A facile synthesis of $SrWO_4$ nanobelts by the sonochemical method. *Mater. Lett.* **2010**, *64*, 2420–2423. [CrossRef]
12. Thongtem, T.; Phuruangrat, A.; Thongtem, S. Preparation and characterization of nanocrystalline $SrWO_4$ using cyclic microwave radiation. *Curr. Appl. Phys.* **2008**, *8*, 189–197. [CrossRef]
13. Gopal, R.; Kumar, A.; Manam, J. Enhanced photoluminescence and abnormal temperature dependent photoluminescence property of $SrWO_4$:Dy^{3+} phosphor by the incorporation of Li^+ ion. *Mater. Chem. Phys.* **2021**, *272*, 124960. [CrossRef]
14. Long, Q.; Xia, Y.; Huang, Y.; Liao, S.; Gao, Y.; Huang, J.; Liang, J.; Cai, J. Na+ induced electric-dipole dominated transition ($^5D_0 \rightarrow {}^7F_2$) of Eu^{3+} emission in $AMgPO_4$:Eu^{3+} (A = Li^+, Na^+, K^+) phosphors. *Mater. Lett.* **2015**, *145*, 359–362. [CrossRef]

15. Roh, H.; Lee, S.; Caliskan, S.; Yoon, C.; Lee, J. Luminescence and electric dipole in Eu^{3+} doped strontium phosphate: Effect of SiO_4. *J. Alloys Compd.* **2019**, *772*, 573–578. [CrossRef]
16. Blasse, G.; Bril, A. Luminescence of Phosphors Based on Host Lattices ABO_4 (A is Sc, In; B is P, V, Nb). *J. Chem. Phys.* **1969**, *50*, 2974–2980. [CrossRef]
17. Song, X.; Wang, X.; Xu, X.; Liu, X.; Ge, X.; Meng, F. Crystal structure and magnetic-dipole emissions of Sr_2CaWO_6: RE^{3+} (RE = Dy, Sm and Eu) phosphors. *J. Alloys Compd.* **2018**, *739*, 660–668. [CrossRef]
18. Yu, R.; Wang, C.; Chen, J.; Wu, Y.; Li, H.; Ma, H. Photoluminescence Characteristics of Eu^{3+}-Doped Double-Perovskite Phosphors. *ECS J. Solid State Sci. Technol.* **2014**, *3*, R33–R37. [CrossRef]
19. Tian, L.; Yu, B.; Pyun, C.; Park, H.L.; Mho, S. New red phosphors $BaZr(BO_3)_2$ and $SrAl_2B_2O_7$ doped with Eu^{3+} for PDP applications. *Solid State Commun.* **2004**, *129*, 43–46. [CrossRef]
20. Yu, P.; Su, L.; Xu, J. Synthesis and Luminescence Properties of Eu^{3+}, Bi^{3+}-Doped BaWO4 Phosphors. *Opt. Rev.* **2014**, *21*, 455–460. [CrossRef]
21. Jung, J.; Kim, J.; Shim, Y.; Hwang, D.; Son, C.S. Structure and Photoluminescence Properties of Rare-Earth (Dy^{3+}, Tb^{3+}, Sm^{3+})-Doped $BaWO_4$ Phosphors Synthesized via Co-Precipitation for Anti-Counterfeiting. *Materials* **2020**, *13*, 4165. [CrossRef]
22. Shinde, K.N.; Dhoble, S.J.; Kumar, A. Combustion synthesis of Ce^{3+}, Eu^{3+} and Dy^{3+} activated $NaCaPO_4$ phosphors. *J. Rare Earths* **2011**, *29*, 527–535. [CrossRef]
23. Qi, G.; Yang, R.T.; Chang, R. MnO_x-CeO_2 mixed oxides prepared by co-precipitation for selective catalytic reduction of NO with NH_3 at low temperatures. *Appl. Catal. B Environ.* **2004**, *51*, 93–106. [CrossRef]
24. Thongtem, T.; Kungwankunakorn, S.; Kuntalue, B.; Phuruangrat, A.; Thongtem, S. Luminescence and absorbance of highly crystalline $CaMoO_4$, $SrMoO_4$, $CaWO_4$ and $SrWO_4$ nanoparticles synthesized by co-precipitation method at room temperature. *J. Alloys Compd.* **2010**, *506*, 475–481. [CrossRef]
25. Shu, Y.; Travert, A.; Schiller, R.; Ziebarth, M.; Wormsbecher, R.; Cheng, W. Effect of Ionic Radius of Rare Earth on USY Zeolite in Fluid Catalytic Cracking: Fundamentals and Commercial Application. *Top. Catal.* **2015**, *58*, 334–342. [CrossRef]
26. Krishna Bharat, L.; Lee, S.H.; Yu, J.S. Synthesis, structural and optical properties of BaMoO4:Eu^{3+} shuttle like phosphors. *Mater. Res. Bull.* **2014**, *53*, 49–53. [CrossRef]
27. Liao, J.; Qiu, B.; Wen, H.; Chen, J.; You, W. Hydrothermal synthesis and photoluminescence of $SrWO_4$:Tb^3+ novel green phosphor. *Mater. Res. Bull.* **2009**, *44*, 1863–1866. [CrossRef]
28. Barja, B.; Baggio, R.; Garland, M.T.; Aramendia, P.F.; Peña, O.; Perec, M. Crystal structures and luminescent properties of terbium(III) carboxylates. *Inorg. Chim. Acta* **2003**, *346*, 187–196. [CrossRef]
29. Tseng, T.; Choi, J.; Davidson, M.; Holloway, P.H. Synthesis and luminescent characteristics of europium dopants in SiO_2/Gd_2O_3 core/shell scintillating nanoparticles. *J. Mater. Chem.* **2010**, *20*, 6111–6115. [CrossRef]
30. Dhara, S.; Imakita, K.; Mizuhata, M.; Fujii, M. Europium doping induced symmetry deviation and its impact on the second harmonic generation of doped ZnO nanowires. *Nanotechnology* **2014**, *25*, 225202. [CrossRef]
31. Sun, S.; Guo, R.; Zhang, Q.; Lv, X.; Leng, P.; Wang, Y.; Huang, Z.; Wang, L. Efficient deep-blue thermally activated delayed fluorescence emitters based on diphenylsulfone-derivative acceptor. *Dye. Pigment.* **2020**, *178*, 108367. [CrossRef]
32. Zhu, H.; Qian, B.; Zhou, X.; Song, Y.; Zheng, K.; Sheng, Y.; Zou, H. Tunable luminescence and energy transfer of Tb^{3+}/Eu^3+ co-doped cubic $CaCO_3$ nanoparticles. *J. Lumin.* **2018**, *203*, 441–446. [CrossRef]
33. Pandey, A.; Rai, V.K.; Kumar, V.; Kumar, V.; Swart, H.C. Upconversion based temperature sensing ability of Er^{3+}–Yb^{3+}codoped $SrWO_4$: An optical heating phosphor. *Sens. Actuators B Chem.* **2015**, *209*, 352–358. [CrossRef]
34. Song, H.; Wang, C.; Han, Q.; Tang, X.; Yan, W.; Chen, Y.; Jiang, J.; Liu, T. Highly sensitive Tm^{3+}/Yb^{3+} codoped $SrWO_4$ for optical thermometry. *Sens. Actuators A Phys.* **2018**, *271*, 278–282. [CrossRef]
35. Li, G.; Gao, S.; He, W. Preparation and photoluminescence properties of the Sm^{3+}, Eu^{3+} co-doped $CaWO_4$ phosphors. *Optik* **2015**, *126*, 3272–3275. [CrossRef]
36. Kang, F.; Hu, Y.; Wu, H.; Mu, Z.; Ju, G.; Fu, C.; Li, N. Luminescence and red long afterglow investigation of Eu^{3+}–Sm^{3+} CO-doped $CaWO_4$ phosphor. *J. Lumin.* **2012**, *132*, 887–894. [CrossRef]
37. Ren, Y.; Liu, Y.; Yang, R. A series of color tunable yellow–orange–red-emitting $SrWO_4$:RE (Sm^{3+}, Eu^{3+}–Sm^{3+}) phosphor for near ultraviolet and blue light-based warm white light emitting diodes. *Superlattices Microstruct.* **2016**, *91*, 138–147. [CrossRef]